A Novel Approach for Solving Nonlinear Flow Equations: A Next Step towards an Accurate Assessment of Shale Gas Resources

Yashar Bezyan [a], Mohammad Ebadi [b,*], Shahab Gerami [c], Roozbeh Rafati [d], Mohammad Sharifi [e], Dmitry Koroteev [b]

[a] Department of Petroleum Engineering, Science and Research Branch, Islamic Azad University, Tehran, Iran

[b] Skolkovo Institute of Science and Technology, Skolkovo Innovation Centre, Moscow, Building 3, Moscow, 143026, Russia

[c] IOR Research Institute, Tehran, Iran

[d] School of Engineering, University of Aberdeen, Aberdeen, United Kingdom, AB24 3UE

[e] Department of Petroleum Engineering, Amirkabir University of Technology, Tehran, Iran

* Corresponding Author: Mohammad.Ebadi@Skoltech.ru

Abstract

As ultra-tight porous media that include organic contents, shale gas resources are technically known as complex systems having various mechanisms that impact storage and flow. The slippage, Knudsen diffusion, the process of desorption, an adsorbed layer that affects apparent permeability, and solute gas in kerogen are recognized to be the most important ones. However, simultaneous effects of multi-mechanism flow and storage, and influences of scattered organic contents on shale gas flow behaviour are not well-understood yet.

According to the mass conservation law, a basic mathematical model has been developed to investigate, step-by-step, the effects of different changes that are introduced, and examine whether patterns of how kerogen is distributed affect the production plateaus. The discretization of the second-order nonlinear Partial Differential Equation (PDE) that is evolved results in a certain number of nonlinear simultaneous algebraic equations, which are conventionally solved with the application of Newton's method. To overcome the inherent difficulties of the initial guess, the derivations, and the inversion of the Jacobian matrix, a new application of Particle Swarm Optimization (PSO) as a nonlinear solver was applied to extract the anticipated pressure profile for each step in time outside the bounds of the reference equations.

The results show that not only can the PSO effectively meet the required criteria, but also it performed faster than conventional techniques, especially in cases with a larger number of grids that encompass more phenomena. It was further revealed that insertion of a multi-mechanism apparent permeability model in which the pore radius is also a pressure-dependent parameter causes the lower rate of production. A higher level of production has been recorded after including storage terms of adsorption and solute gas in kerogens. Although different patterns of kerogen distribution have finally overlapped, different taken trend of each production profile underlines the impact of kerogen distribution as an important parameter within the procedure of history matching.

Key words:

Shale gas reservoirs; apparent permeability; adsorbed gas; kerogen distribution; Newton's method; Particle Swarm Optimization

Nomenclature

Δx	Length of Each Grid; *ft*
A	Surface Area; ft^2
A_K	Kerogen Surface Area; ft^2
C	Net Heat of Adsorption; *Dimensionless*
c	Concentration; lb_m / ft^3
C_g	Gas Compressibility; psi^{-1}
d	Pore Diameter; *ft*
D	Kerogen Diffusivity Coefficient; ft^2/Day
D_f	Surface Roughness; *Dimensionless*
d_m	Normalized Molecular Size; *ft*
E_1	Heat of Adsorption for the First Layer; *Dimensionless*
E_L	Heat of Higher Layers; *Dimensionless*
k	Absolute Permeability; *md*
K_a	Differential Equilibrium Partitioning Coefficient; *Dimensionless*
k_{app}	Apparent Permeability; *md*
k_H	Henry's Constant; $lb/(psi\text{-}ft^3)$
K_n	Knudsen Number; *Dimensionless*
M	Molecular Weight; lb_m
n	Number of Gas Moles; *lb mol*
P	Pressure; *psi*
P_{cte}	Constant Pressure; *psi*
P_{in}	Initial Pressure; *psi*
P_L	Langmuir Pressure; *psi*
P_o	Saturation Pressure of the Gas; *psi*
P_{ST}	Standard Pressure; *psi*
q_k^*	Mass Flux from kerogen to Matrix (Kerogen Mass Flux); lb_m / day

R Gas Constant; $(psi.ft^3)/(lb\ mol\ .\ ^\circ R)$

r Pore Radius; ft

r_{eff} Effective Pore Radius; ft

r_{mol} Radius of Gas Molecules; ft

T Temperature; $^\circ F$

t Time; day

t_{ads} Thickness of the Adsorbed Layer; ft

T_{ST} Standard Temperature; $^\circ F$

V Gas Volume of Adsorption; ft^3 / lb_m

V_b Bulk Volume; ft^3

V_L Langmuir Volume; ft^3 / lb_m

V_m Maximum Volume of Adsorbed Gas for a Single Molecular Layer; ft^3 / lb_m

Z Compressibility Factor; *Dimensionless*

z Height; ft

Greek Letters

α Adsorbed Layer Fitting Slope; ft / psi

δ' Size Ratio; *Dimensionless*

ζ Tangential Momentum Accommodation Coefficient; *Dimensionless*

λ Mean Free Path; ft

μ Viscosity; cp

ρ_a Density of Adsorbed Gas; lb_m / ft^3

ρ_{avg} Averaged Density; lb_m / ft^3

ρ_b Bulk Density; lb_m / ft^3

ρ_f Density of Free or compressed Gas; lb_m / ft^3

ρ_s Density of Solute Gas; lb_m / ft^3

τ Tortuosity; *Dimensionless*

υ Darcy's Velocity; (ft / day)

ϕ Porosity; *Dimensionless*

1. Introduction

Shale gas resources, which are discussed on a daily basis, have drawn many researchers' attentions towards the new wonder of "The Shale Gas Revolution". This slowly growing movement started the century by compromising just less than 2 percent of domestic outputs. Surprisingly, today it accounts for nearly one-third, and the projection is that by 2030s is a half of the gas produced in the USA and China will be from shale gas resources [1]. Recent industrial and scientific advances have caused experts conclude that organic-rich shales have the potential to be regarded not only as sources containing of typical oil and gas, but also as reservoirs to be produced [2].

Applying modern methods like high pressure mercury injection (up to 60000 psi) and novel photo techniques have proved the existences of nano scale pores and throats in organic-rich shale gas resources [3, 4]. Nano scale pores have strong effects on the storage and flow in shale gas resources. First, they provide large exposed surface areas known to hold the potential for a considerable amount of adsorbed gas. Also, Darcy's law is not applicable to shale gas resources because it has originally been developed for micro scale pores [3-10]. Moreover, the trapped organic content, kerogen, is also one of the other most special and unique characteristics of shale gas resources that has an impact on the storage and flow of gas [4, 11, 12].

Last relevant research has discovered that the organic constituents cover part of the bulk rock, and are irregularly distributed in the shale gas media. Dispersed organic materials within the shales can affect flow and storage mechanisms [5, 12-15]. Specifically, gas is typically stored in pores, and adsorbed on the oil-wet surface of nano scale pores on organic contents that can also

have noticeable effects on the non-Darcy's flow [16-19]. On the contrary, the water-wet nature of clays caused the provided empty sites to be filled with water. Therefore, it has been concluded that a notable fraction of the adsorbed gas is stored in the kerogen pores [12, 20, 21]. Besides that, more research has indicated that a portion of gas molecules remain in the solid part of the organic matter in the form of solute gas. Indeed, scattering of the kerogen is the substantial parameter that has a great impact on modelling and simulation of storage and flow in the shale gas resources [5, 12-15].

To describe the fluid flow of gas as a compressible fluid in conventional porous media, the benefits of Darcy's equation have been combined with the continuity equation. The strong functionality of gas parameters such as density, viscosity, and Z-factor on the pressure is the main reason why the supposed governing equation is presumed to be a nonlinear partial differential equation (PDE). In addition, the inclusion of other pressure-dependent phenomena with shale gas resources like apparent permeability, adsorption, and the release of gas from kerogen bodies lead the supposed second-order PDE towards a higher level of nonlinearity [24]. Undoubtedly, handling the nonlinear equations is one of the most challenging problems in numerical computations. Although there are possibilities of applying linearization techniques, the generation of results which are not satisfyingly accurate enough is the main reason to use methods which can directly solve the supposed nonlinearity. Among the different conventional techniques that have ever been proposed to solve the equations referred to, Newton's method is undoubtedly the one that is the most extensively used [25].

However, performance and convergence for Newton's algorithm is strongly dependent on the proper initial guess. Also, the heavily derivation-dependent, high computational cost of Jacobian matrix, and lack of ability to deal with ill-conditioned matrixes, are known to be other

disadvantages [25, 26]. Therefore, researchers' attentions have been drawn towards proposing more advanced methods that meet the required level of accuracy, and with less computational cost for solving the nonlinear problems [27, 29]. Particle swarm optimization (PSO) as an evolutionary and modern optimizer, which can find the optimal solution in the space that is being searched, has recently been proposed to deal with the nonlinearity of different engineering problems [30, 31]. Although there are some couple of research in which the PSO has been applied to solve nonlinear equations, the current research has taken advantages of PSO to solve a certain number of nonlinear simultaneous algebraic equations generated after the discretization of the supposed PDE.

In more details, a basic conventional Darcy's law has been modified to account for the effect of slippage, Knudsen diffusion, and impacts of adsorbed layer on the apparent permeability. Moreover, gas desorption from the pore walls and effects of solute gas in bulks of kerogens are considered to correct the accumulation term. While the generated nonlinear simultaneous algebraic equations generated have been conventionally solved, the applicability of PSO as a free-derivation solver has also been investigated. At the final step, the positions of organic matters and their distribution effects on the fluid flow behaviour was investigated numerically.

2. Relevant Phenomena to Shale Gas

The considerable dissimilarities among shale gas reservoirs with conventional oil and gas resources due to the existence of organic contents and natural nano scale pores, have been analysed in brief.

2.1 Multi-Mechanism Flow and Apparent Permeability

Generally, using conventional continuum flow equations and Darcy's law underestimate the flow rate when used for the ultra-tight porous media of shale gas resources. That is due to the assumption of zero-velocity boundary condition [8, 32-36]. To figure out the concept of multi-mechanism flow in ultra-tight porous media, the Knudsen number (K_n) is normally considered to be a clarifying index [3]. The various flow regimes can be identified as:

$$K_n = \frac{\lambda}{d} \tag{1}$$

where λ in shale gas reservoirs is physically defined as the average distance travelled by a gas molecule before colliding with another molecule that changes its energy, track, or other properties [37]. Classifications of flow regimes based on K_n, and the relevant information and highlights have been reported in **Table 1**.

Insert Table 1

Detailed studies about the morphology and pore size distribution of shale gas reservoirs show that the pore sizes in the shales under study ranges from 1 to 200 nm, resulting in the generation of K_n relaying between 0.0002 and 6, respectively [41-43]. Altogether, it can be deduced that flow in shale gas reservoirs is a multi-mechanism phenomena including continuum flow, slip flow, and transition flow [34, 40]. The topic under discussion about flow in shale gas reservoirs, and relevant complexities, has been graphically depicted in **Figure 1**.

Insert Figure 1

There is an enlarged thin section of shale gas matrixes that includes different ranges of pore sizes leading to the generation of various K_n, and their corresponding flow regimes as well.

According to previous studies on characterizing of flow in ultra-tight porous materials, the first classic apparent permeability model specific for shale gas resources was proposed by Javadpour [4]. This model describes the multi-mechanism flow in the bundle of nano tubes based on pressure forces and Knudsen diffusion. More details are described in **Table 2**. The opportunity for advancements in order to make the former model more suitable for porous media was taken by Darabi et al. [8]. Porosity, permeability and tortuosity as the main characteristic of a typical porous media was incorporated into the previous model. The new model accounts for some complexities in gas flow through ultra-tight natural porous media. For example, local heterogeneity is one of the main factors which is routinely ignored in previous models, but it was inserted into the new model, with satisfying results.

Insert Table 2

2.2 Adsorbed Gas

Calculations of gas-in-place in shale gas reservoirs have repeatedly been reported as a challenging issue. That is due to the fact that the final volume is not only a function of compacted free gas, but is also intensively influenced by what is adsorbed on the surface of kerogens [5, 16], **Figure 2**.

Insert Figure 2

In other words, disregarding the adsorbed gas having a semi-liquid physical state with greater density than the free compressed gas leads to some remarkable underestimation. The effects of the adsorbed gas can become more pronounced when they accompany with the noticeable amount of surface area in shale gas reservoirs that is exponentially larger than what it is in conventional reservoirs [5, 7, 44, 45]. Specifically, the pore structure and TOC are the most important parameters affecting adsorption, although other factors like depth, temperature,

moisture, and pressure can have their own importance [45-47]. Through consideration of a dynamic instantaneous equilibrium at a constant pressure and temperature between non-adsorbed and adsorbed gas, the classic Langmuir isotherm is the most common adsorption isotherm that is routinely used [44-46]. More details can be found in **Table 3**. Some challenges such as the simplicity of the monolayer adsorption assumption of gas molecules at high pressures have also been taken as excuses to apply other models like BET [48].

Insert Table 3

Also, the gas molecules which stick to pore surfaces, known as adsorbed layer, limit the available conductance for the flow of free and already desorbed gas. Subsequently, the adsorbed gas has a negative effect on permeability, since the methane molecule radius is comparable to the pore sizes.

On the other hand, below a certain critical pressure the adsorbed molecules begin to be desorbed. In fact, gas molecule desorption occurring due to the pressure reduction decreases the thickness of adsorbed layer, which results in an improvement for permeability. The significance of the adsorbed layer on the flow path properties has led recent research to predict the thickness of adsorbed gas molecule according to alteration in pressure [9, 49-51]. Some couple of relevant research is shown brief in **Table 4**.

Insert Table 4

2.3 Kerogen

Kerogen is the organic material analogous to the bitumen that has the capability of storing hydrocarbons in a dissolved state. Recent researches have theoretically and experimentally been reported that a noticeable part of the gas-in-place in shale reservoirs is in the form of a solute

stored in the kerogen [4, 18, 20, 52]. It also states that the solute gas could contribute to the total gas production when an imbalance in concentration is created between the gas on the surface and within the kerogen bulk owing to the gas desorption [4]. Even so, few studies have been conducted on the gas transport mechanism in kerogen medium. Most of the scientists believe that gas production from kerogen is a slow process and Fickian flow is the predominant transport mechanism. The second law of Fick in the Cartesian coordinate and z-direction is represented as [22, 53-56]:

$$\frac{\partial^2 c}{\partial z^2} = \frac{1}{D}\frac{\partial c}{\partial t} \tag{2}$$

where c is concentration, D is the diffusion coefficient, and z and t represent the space and time, respectively.

3. Methodology

The current study considers a comprehensive model in which a variety of flow and storage mechanisms occur in a mathematical model of the organic-rich shale. Pressure reduction due to the production of free gas molecules causes desorption of molecules stuck on the surface of kerogen. The latter causes a disturbance in the system, leading to the creation of a concentration gradient between the pore walls and bodies of kerogens. This will be the main reason for the transmission of solute gas from the bulk of a kerogen to its surfaces. The arrangement is schematically presented in **Figure 3**.

Insert Figure 3

In particular, the block under study includes a non-organic part known as clay which has no effects on the main flow of gas molecules. The green sign indicates the direction of the main non-Darcy flow of free molecules (red) and those which have already been desorbed (blue) due

to the pressure reduction. The gas molecules flow from a no-flow boundary towards a constant pressure mode. Of course, there is an organic part known as kerogen containing solute gas (yellow). Black signs show the diffusion of solute gas molecules towards the interface between kerogen and pore space. The procedure has been symbolized with bicoloured circles. The multi-mechanism process that is pictured was developed in gradual steps from a basic model towards an advanced one representing a shale gas system.

3.1 Model Description

Through taking advantages of the conservation mass equation for a single grid, a one-dimensional (1D) model of a conventional porous media can be developed as [24]:

$$-\left(\left(\rho_f vA\right)_{x+dx}\Delta t-\left(\rho_f vA\right)_x\Delta t\right)=V_b\phi\left(\left(\rho_f\right)_{t+dt}-\left(\rho_f\right)_t\right) \quad (3)$$

It can be rearranged as:

$$-\frac{\partial\left(\rho_f vA\right)}{\partial x}\Delta x=V_b\frac{\partial}{\partial t}\left(\phi\rho_f\right) \quad (4)$$

where υ is Darcy's velocity and defined as:

$$v=-(5.615)(0.001127)\frac{k}{\mu}\frac{\partial p}{\partial x} \quad (5)$$

Combining **Equation 5** and **Equation 4** yields [24, 57]:

$$\frac{\partial}{\partial x}\left(0.00633\,kA\frac{\rho_f}{\mu}\frac{\partial P}{\partial x}\right)\Delta x=\frac{\partial}{\partial t}V_b(\rho_f\phi) \quad (6)$$

where k is absolute permeability, A is the cross-section area, $\rho_f$is free gas density, μ is gas viscosity, P is pressure, Δx is the length of each grid, t is time, V_b is the bulk volume and ϕ is the porosity. Specifying an initial and two boundary conditions is necessary to find a solution for **Equation 6**. For the initial condition, it is assumed that the pressure is uniform and stable all over the model before production begins. One side of the 1D sample is faced with a constant

pressure boundary, which is mathematically recalls the Dirichlet situation, in which the flow rate is dynamic and the constant pressure plays the role of a chock. On the other hand, the sample is controlled by a Neumann state with a no-flow boundary or isolation condition. These conditions can be mathematically translated as [22, 50]:

$$Initial\ Condition: \quad P = P_{in} \quad @\ t = 0; \quad 0 < x < L$$

$$Left\ Boundary\ Condition: \quad P = P_{cte} \quad @\ t > 0; \quad x = 0$$

$$Right\ Boundary\ Condition: \quad \frac{\partial P}{\partial x} = 0 \quad @\ t > 0; \quad x = L$$

3.2 Fluid Flow Equation

In order to obtain the proper model for unconventional shale gas reservoirs, the basic model has been combined with flow and storage characteristics of shale gas resources that have already been discussed. To simulate and consider the effect of slippage and diffusion in nano pores, the absolute permeability has been replaced with apparent permeability, **Equation 7** [4, 8].

$$\frac{\partial}{\partial x}\left(0.00633 k_{app} A \frac{\rho_f}{\mu} \frac{\partial P}{\partial x}\right) \Delta x = \frac{\partial}{\partial t} V_b (\rho_f \phi) \tag{7}$$

where k_{app} is the apparent permeability. It is calculated based on the model proposed by Darabi et al. [8]. Besides compressed gas in the pore voids, adsorbed gas on pore walls is considered to be another type of storage (accumulation). Therefore, **Equation 7** is turned into [8, 48, 58]:

$$\frac{\partial}{\partial x}\left(0.00633\, k_{app} A \frac{\rho_f}{\mu} \frac{\partial P}{\partial x}\right) \Delta x = \frac{\partial}{\partial t} V_b \left(\rho_f \phi + (1-\phi)\rho_a\right) \tag{8}$$

where ρ_a is the density of the adsorbed gas (the mass of adsorbed gas per volume of solid). Chain rule and compressibility definition are employed to find a simple expression for the right side. Mathematically, it can be stated as [24, 58]:

$$C_g = \frac{1}{\rho_f}\frac{\partial \rho_f}{\partial P} \tag{9}$$

$$\frac{\partial \rho_f}{\partial t} = \frac{\partial \rho_f}{\partial P}\frac{\partial P}{\partial t} = C_g \rho_f \frac{\partial P}{\partial t} \tag{10}$$

where C_g is the gas compressibility. For the second term, it can be presented mathematically as [48, 58]:

$$\frac{\partial \rho_a}{\partial t} = \frac{\partial \rho_a}{\partial \rho_f}\frac{\partial \rho_f}{\partial P}\frac{\partial P}{\partial t} = \frac{\partial \rho_a}{\partial \rho_f} C_g \rho_f \frac{\partial P}{\partial t} \tag{11}$$

Based on **Equations 10** and **11**, **Equation 8** can be reformed as [8, 41, 60]:

$$\frac{\partial}{\partial x}\left(0.00633\, k_{app}\, A \frac{\rho_f}{\mu}\, \frac{\partial P}{\partial x}\right)\Delta x = \frac{\partial P}{\partial t} V_b C_g \rho_f \left(\phi + (1-\phi)\frac{\partial \rho_a}{\partial \rho_f}\right) \tag{12}$$

Moreover, Patzek et al. [59] defined the differential equilibrium partitioning coefficient of gas at a given temperature as:

$$K_a = \frac{\partial \rho_a}{\partial \rho_f} \tag{13}$$

Taking the advantages of **Equation 13** causes **Equation 12** to be formed as [48, 58]:

$$\frac{\partial}{\partial x}\left(0.00633\, k_{app}\, A \frac{\rho_f}{\mu}\, \frac{\partial P}{\partial x}\right)\Delta x = \frac{\partial P}{\partial t} C_g \rho_f V_b (\phi + (1-\phi)K_a) \tag{14}$$

In order to obtain a mathematical expression for ρ_a and its derivative, the mass balance of adsorbed gas is formed as [48]:

$$\rho_a V_b (1-\phi) = \rho_f(P_{ST}, T_{ST}) \rho_b V_b V \tag{15}$$

where $\rho_f(P_{ST}, T_{ST})$ represents gas density in standard conditions, and V is volume of adsorbed gas per bulk volume of the rock. Rearrangement of the latter equation results in:

$$\rho_a = \frac{\rho_f(P_{ST}, T_{ST})\rho_b}{(1-\phi)} V \tag{16}$$

Since the adsorbed molecules occupy a portion of the flow path, it is necessary to modify the pore diameter during the procedure of desorption. The alteration within the thickness of the adsorbed layer, and the subsequent effects on the apparent permeability, has been modelled based on the following:

$$r_{eff} = r - t_{ads} \tag{17}$$

where r_{eff} is the effective pore radius, r is the pore radius, and t_{ads} is the thickness of the adsorbed layer. The thickness of the adsorbed layer responds according to what has been represented by Sakhaeepour and Braynt [49] in **Table 4**.

Besides that, it is assumed that the solute gas obeys **Equation 2**, and diffuses linearly in the z direction within the kerogen body. The quantity of the gas that is solute in the kerogen can be calculated according to Henry's law, in which the solute gas is proportional to the pressure of the gas in the pore, which is represented as [22, 54, 60]:

$$c = k_H P \tag{18}$$

where k_H is Henry's constant, and P is pressure. To solve **Equation 2,** the initial and boundary conditions have been set. The supposed initial condition is given as below:

$$Initial\ Condition: \quad c_{in} = k_H P_{in} \quad @t = 0; \quad 0 \le z \le h$$

The interface between the kerogen and pore wall is considered to be the inner boundary at z = 0 where the gas concentration in the element under study would be:

$$Boundary\ Condition\ 1: \quad c = k_H P; \quad z = 0; \quad t > 0$$

The outer body of kerogen is surrounded by clay minerals which cannot feed gas molecules. Accordingly, the no-flow boundary is set for the outer boundary of the kerogen at z = h which can mathematically be presented as [22, 53, 54, 56]:

$$Boundary\ Condition\ 2: \quad \frac{\partial c}{\partial z} = 0; \quad z = h; \quad t > 0$$

Eventually, rate of mass transfer between kerogen and pore space can be calculated by [22, 54]:

$$q_k^* = D_k . A_k . \frac{\partial c}{\partial z} \tag{19}$$

where q_k^* is kerogen mass flux, D_k is kerogen diffusion coefficient, and A_k is kerogen surface area. To consider the effect of kerogen q_k^*, it is inserted as a source term to the left side of the equation. Furthermore, it has notably been discussed that the dimensions of kerogens are 10 times greater than pore sizes [22, 54, 55]. It must be remembered that the introduced term has originally been inspired from fractured reservoirs, technically known as double-porosity media. Accordingly, after the insertion of **Equation 19** into the main **Equation 14**, the final form of the governing partial differential equation is [22, 54, 60]:

$$\frac{\partial}{\partial x}\left(0.00633\, k_{app}\, A \frac{\rho}{\mu} \frac{\partial P}{\partial x}\right) \Delta x + q_k^* = \frac{\partial P}{\partial t} V_b C_g \rho_f (\phi + (1-\phi) K_a) \tag{20}$$

Equation 20 is the mathematical expression of what is happening in **Figure 3**.

3.3 Solver

To numerically solve the resulted governing equation, the application of discretization based on the finite difference method generates standard simultaneous equations. It can mathematically be stated as:

$$[Coeff.][P] = 0 \tag{21}$$

where *[Coeff.]* represents the matrix of coefficients and *[P]* is the matrix of unknown pressures. By regarding the thermodynamical nature of gases, the produced simultaneous equations that are produced are nonlinear. Usually, the Newton's method which takes advantages of the Jacobian matrix is employed to solve simultaneous nonlinear equations [24]. It is technically performed as [25]:

$$[P_{new}] = [P_{old}] - J^{-1}[f(P_{old})] \tag{22}$$

in which J^{1} is the inversion of the Jacobian matrix, $f(P_{old})$ represents the responses of nonlinear simultaneous algebraic equations, P_{old} is the pressure within the last iteration and the P_{new} symbolizes adjusted pressures. In the Jacobian matrix, each row represents one block and the columns stand for corresponding derivations based on existing variables. Technically, the Jacobian matrix is the matrix of all first-order partial derivatives of a vector-valued function. It is mathematically defined as [25]:

$$J = \frac{df}{dx} = \left[\frac{\partial f}{\partial x_1} \cdots \frac{\partial f}{\partial x_n}\right] = \begin{bmatrix} \frac{\partial f_1}{\partial x_1} & \cdots & \frac{\partial f_1}{\partial x_n} \\ \vdots & \ddots & \vdots \\ \frac{\partial f_m}{\partial x_1} & \cdots & \frac{\partial f_m}{\partial x_n} \end{bmatrix} \tag{23}$$

It must be considered that the quality of the initial guess has a significant impact on the convergence of Newton's method. However, there are some situations in which that arrangement of the Jacobian matrix is somehow unmanageable [25]. For instance, it is understood that forming the Jacobian matrix needs to have the derivations for pressure-dependent parameters. Some of parameters like apparent permeability can be subjected into both classical and numerical derivations. Choosing between one of these two is challenging because developing these classical methods are time-consuming, and the numerical ones have inherent errors. On the other hand, for parameters like the Z-factor, which is supposed to undergo numerical derivation while choosing one of the methods of backward, central, or forward causes that generate of different results again [24, 25]. Moreover, the computational cost of Newton's method is also considerable because the inversion of the Jacobian matrix must be calculated for a certain number of iterations in each time step.

To overcome the addressed challenges of the initial guess and the relevant difficulties with the Jacobian Matrix, the PSO as a free derivation technique which does not need to have an initial

guess can conclude the group of pressures, which their product with the matrix of coefficients in each time step generate a relative zeros matrix [30, 31, 61].

In short, PSO is a stochastic optimization technique inspired by social systems among organisms such as birds flocking and fish schooling. This robust technique which has recently drawn many petroleum researchers' attentions, can effectively be employed to solve multidimensional optimization problems [62-67]. Starting with a set of random particles or potential solutions including the numbers of pressures, the algorithm makes attempts to improve solutions based on their corresponding qualities, which ideally generates a certain number of zeros. To iteratively reach the supposed goal, each particle changes its values by using velocity vectors that are altered with the effects of random factors. The procedure can mathematically be stated as [68]:

$$x_{i,j}^{k+1} = x_{i,j}^{k} + v_{i,j}^{k+1} \tag{24}$$

where

$$v_{i,j}^{k+1} = v_{i,j}^{k} + c_1 r_1 \left({x_{lbest}}_{i,j}^{k} - x_{i,j}^{k} \right) + c_2 r_2 \left({x_{gbest}}_{i,j}^{k} - x_{i,j}^{k} \right) \tag{25}$$

r_1 and r_2 are uniformly distributed random numbers within the range of 0 to 1. In the *k*th iteration, $v_{i,j}^{k}$ and $x_{i,j}^{k}$are the *j*th component of the *i*th particle's velocity and position vector, respectively. Also, x_{lbest} and x_{gbest} reflect the best positions experienced so far by the *i*th particle and the whole population as well. Moreover, c_1 and c_2, show each particle's confidence in itself and in the population, correspondingly [68]. The applied values for the relevant parameters of PSO have been laid out in **Table 5**.

Insert Table 5

Graphically, the proposed procedure has been indicated in **Figure 4,** where the functionality of the PSO has been performed step by step.

Insert Figure 4

4. Results and Discussions

Based on the initial values of the parameters stated in **Table 6**, the basic homogenous model which has mathematically been introduced with **Equation 6** was solved by applying Newton's and PSO methods.

Insert Table 6

The generated production results have been presented in **Figure 5,** where they have been compared against outputs from the analytical solution of the pictured model addressed in well-known references [69]. According to the statistical parameters of R-square (R^2) and Minimum Square Error (MSE), the developed model applied with the both numerical methods satisfyingly performed in keeping with the analytical outputs. In terms of computational time, it can also be inferred that there is not a very broad difference between both applied solvers, and they perform nearly the same.

Insert Figure 5

By regarding the model for apparent permeability proposed by Darabi et al. [8], and what has been described about the phenomena of adsorption under the title of the Langmuir isotherm, it is possible to analyse **Equation 14** based on applying the solvers being referred to. The effects of inserting the apparent permeability, which symbolizes the slippage and Knudsen diffusion, and the desorption process on the production profile, are shown in **Figure 6**.

Insert Figure 6

To examine the effects of the adsorbed layer on the trend of apparent permeability, the model proposed by Darabi et al. [8] has been coupled with what was suggested by Sakhaee-pour and Bryant [49]. Specifically, the radius referred to in the presumed apparent permeability model turns into a function of pressure based on a linear relationship. The results are vividly apparent in the first part of **Figure 7**. The thickness of the adsorbed layer has been assumed as what was mentioned in **Table 4**. Below the 4061 psi, the effective flow path gradually becomes enhanced until the gas molecules on the pore walls are entirely desorbed. Ultimately, if lower than the 500 psi pressure, the adsorbed layer has a negligible effect, and causes the effective flow path and intrinsic pore diameter to become identical.

The second part represents the importance of adsorbed layer effects on the production profile in comparison with the exclusion of the considering effect and apparent permeability model solely without any second storage mechanism. At the early time of production, the trend of inclusion has lower production rather than both cases. It can be labelled so that the lower amounts of desorption process at the beginning of the production leads to a thicker adsorbed layer. It means that the flow path at the beginning has a smaller size than what it really is. As production continues, the desorption process accelerates, and the adsorbed layer starts to diminish. Eventually, at a later time, since the total gas in place is identical, both trends are going to meet each other and reach a peak of cumulative production, although they followed different paths.

Adding the adsorbed layer to the previously discussed phenomena, apparent permeability and desorption, amplifies the level of complexities which can noticeably, effectively, and robustly be overcome by applying the PSO method shown in the third part. While implementing Newton's method as a conventional technique takes as long as 151 seconds in the highest number of grids, this proposed solver only needs 112 seconds.

Insert Figure 7

The process of evolution for the basic model approaches towards the final step by including the effects of solute gas stored in kerogens. Impacts of the solute gas stored in organic contents on production profiles are illustrated in Figure 8 (a). It can clearly be observed that inserting solute gas effects causes a significant jump in the level of stabilization, or the amount of gas produced, which follows previous expectations about gas-in-place assumptions. With this in mind, it can be concluded that solute gas effects play a leading role in the reserve estimations, and discounting it leads to be faced up with significant errors. Moreover, including the effects of solute gas results in a dramatic shift in stabilization. While the developed model without solute gas effects stabilize after 4 days, the fully developed model levels off after 14 days which shows the slow process of diffusion within kerogen bodies. There is also another trend that includes the solute gas effects but disregards the importance of the adsorbed layer. Without the adsorbed layer, the surface of kerogen is affected more readily due to the higher permeability that has already been shown in **Figure 7**. The faster process for depletion within the kerogen starts, and less time is required to reach the peak of the cumulative production. In the second part of **Figure 8**, the fully developed model has been subjected to two different solvers. As can be understood, less time is required to solve the presumed nonlinear equations, even in a small number of grids, when the PSO technique is applied.

Insert Figure 8

The overall results of applying the PSO algorithm as a solver in comparison with the conventional method, in terms of computational time, are illustrated in **Table 7.** The time spent with the PSO and Newton's to solve the required simultaneous equations are represented in red and blue, respectively. Based on the fact that both techniques nearly require equal time for a

basic model including different numbers of girds, it can be inferred that applying the PSO for normal cases can be a noticeable plus. It is clear that adding different items into the basic model for the lowest number of grids causes the recording of various computational time with the difference of 60%. However, the robustness of PSO can be vividly highlighted when a complex model includes grids as large as 500, in which the PSO has recorded 124 seconds, which is 31% less than what has already been spent by implementing Newton's method. Interestingly, it is also possible to conclude that complexity and heterogeneity of the model under study does not have the highest level of impact on the amount of computational time. In fact, the tabulated performances of both implemented solvers show that having 400 grids in the most complex case, last row, requires shorter time than having 500 grids, excluding solute gas effects. In other words, increasing in the number of nonlinear simultaneous algebraic equations takes shorter computational time than making the supposed system more complex by inclusion of more phenomena.

Insert Table 7

Furthermore, it was decided to investigate whether the trend showing cumulative production is a function of kerogen distribution. During four different scenarios, with an equal amount of total gas in place, one segment included the kerogen with the relevant phenomena of desorption, gas diffusion, and effects of an adsorbed layer, while the other three segments are only an ultra-tight porous media with the related special effects of apparent permeability. In other words, the length of the physical model (**Figure 3**) was divided equally into 4 main segments, and under each scenario only one segment contains kerogen. The results are illustrated in **Figure 9**.

Insert Figure 9

Within each pattern, the considered segment is assigned with the kerogen, and the remaining ones have a clay matrix. Technically, the higher production in the first segment during the earlier time period can be excused due the fact that the first segment has the kerogen source. It means that the signal of pressure reduction reaches the adsorbed layer more quickly, which causes the beginning of desorption and an improvement in apparent permeability. This is due to the reason that the desorption process causes the adsorbed layer to become thinner, which directly causes the effective pore radius to become larger in size and has a positive influence in terms of approaching towards a larger value for apparent permeability. After that, the signal being referred to starts triggering the kerogen body to initiate the depletion process. After a certain amount of time passes so that the pressure of the last grid in the physical model has become equal to the presumed Dirichlet boundary condition, and there is no more solute gas in the kerogen body, the corresponding production profile starts to stabilize. The position of kerogen with more distance from the outlet causes receiving the signal to be received at a later time, even though the same described chain reactions are going to happen. Although the final value of cumulative production is the same for all scenarios, it can be concluded that kerogen distribution has an important effect on the production profile, and it could generally be determined as an effective parameter in a history matching procedure.

5. Conclusion

In this study, a multi-mechanism conceptual model was developed to investigate the effects of non-Darcy's flow, desorption, adsorbed layer impact, gas diffusion from kerogen bodies and kerogen distribution on the production of shale gas reservoirs. A smart optimization approach has also been introduced to solve the supposed nonlinear simultaneous algebraic equations.

The adsorption phenomena, which mainly occur on the pore walls of organic media, increases the cumulative gas production, although it has also a negative side effect on permeability for the ultra-tight porous media. In other words, the reduction in permeability, due to the existence of adsorbed layer, hinders bringing up total production to the maximum value. Furthermore, it is assumed that the monolayer of adsorbed gas covers the pore surfaces.

Solute gas in kerogen bodies contributes to the total gas production. Kerogen has substantial effects on transportation and storage phenomena of shale gas reservoirs. Desorption and gas diffusion from a kerogen body to its surfaces are the mainly relevant phenomena with organic materials. Various distribution of kerogen creates different production profiles, which makes it an important parameter in history matching for shale gas reservoirs.

PSO as a modern optimizer is a smart and robust technique to solve nonlinear simultaneous algebraic equations. In comparison to Newton's method, PSO is a free derivation solver with a lower computational cost which is also independent to initial guess. Furthermore, it converges faster to the solution, and it is more striking when smaller steps of discretization are chosen and complex phenomena are inserted into the governing equation that increase the nonlinearity of the system.

The developed model can be taken to study multi-dimensional systems with effects of multi-phase flow. Also, its advantages can be taken to do detailed and deep research about the behaviour of compositional systems in ultra-tight porous media. The effect of gravity is another aspect that can easily be introduced into the extended model. Several of addressed issues that have been addressed can be considered for future studies.

References:

[1] Holditch SA. Unconventional oil and gas resources development- Let's do it right. *Journal of Unconventional Oil and Gas Resources* 2013; 1-2: 2-8

[2] Speight JG. Shale Gas Production Processes. Gulf Professional Publishing. 1st ed. Elsevier; 2013.

[3] Javadpour F, Fisher D, Unsworth M. Nanoscale Gas Flow in Shale Gas Sediments. *Journal of Canadian Petroleum Technology* 2007; 46(10): 55-61.

[4] Javadpour F. Nanopores and apparent permeability of gas flow in mudrocks (shales and siltstone). *Journal of Canadian Petroleum Technology* 2009; 48(8): 16–21.

[5] Ambrose RJ, Hartman RC, Diaz-Campos M, Akkutlu IY, and C. H. Sondergeld. Shale Gas-in-Place Calculations Part I: New Pore-Scale Considerations. *SPE Journal* 2012; 17(1): 219–29.

[6] Fathi E, Akkutlu IY. Matrix Heterogeneity Effects on Gas Transport and Adsorption in Coalbed and Shale Gas Reservoirs. *Transport in Porous Media* 2009; 80(2): 281–304.

[7] Cui X, Bustin AM, Bustin RM. Measurements of gas permeability and diffusivity of tight reservoir rocks: Different approaches and their applications, *Geofluids* 2009; 9(3): 208–23.

[8] Darabi H, Ettehad A, Javadpour F, Sepehrnoori K. Gas flow in ultra-tight shale strata. *Journal of Fluid Mechanics* 2012; 710:641–58.

[9] Singh H, Javadpour F, Ettehadtavakkol A, Darabi H. Nonempirical apparent permeability of shale. *SPE Reservoir Evaluation & Engineering* 2013; 17(3): 414–24.

[10] Kang SM, Fathi E, Ambrose RJ, Akkutlu IY, and Sigal RF. Carbon Dioxide Storage Capacity of Organic-Rich Shales. *SPE Journal* 2011; 16(04): 842-55.

[11] Hashmy KH, Abueita S, Barnett C, Jonkers JH. Log-based identification of sweet spots for effective fracs in shale reservoirs. *SPE Canadian Unconventional Resources Conference*, Calgary, Canada; 2011.

[12] Yan B, Wang Y, Killough JE. Beyond dual-porosity modeling for the simulation of complex flow mechanisms in shale reservoirs. *Computational Geosciences 2016*; 20(1): 69–91.

[13] Akkutlu IY, Fathi E. Multiscale gas transport in shales with local kerogen heterogeneities. *SPE Journal* 2012; 17(4): 1002 - 11.

[14] Wasaki A, Akkutlu IY. Permeability of organic-rich shale. *SPE Journal* 2015; 20(6): 1384–96.

[15] Silin D, Kneafsey T, Berkeley L. Shale Gas : Nanometer-Scale Observations and Well Modelling. *Journal of Canadian Petroleum Technology* 2012; 51(6): 464–75.

[16] Haghshenas B, Clarkson CR, Chen S. New Models for Reserve Estimation and Non-Darcy Gas Flow in Shale Gas Reservoirs. *SPE/EAGE European Unconventional Resources Conference and Exhibition*, Vienna, Austria; 2014.

[17] Swami V, Settari A, Javadpour F. A Numerical Model for Multi-Mechanism Flow in Shale Gas Reservoirs with Application to Laboratory Scale Testing. *EAGE Annual Conference & Exhibition incorporating SPE Europec*, London, UK*;* 2013.

[18] Ross DK, Bustin RM. The importance of shale composition and pore structure upon gas

storage potential of shale gas reservoirs. *Marine and Petroleum Geology* 2009; 26(6): 916–27.

[19] Passey QR, Bohacs KM, Esch WL, Klimentidis, Sinha S. From Oil-Prone Source Rock to Gas-Producing Shale Reservoir - Geologic and Petrophysical Characterization of Unconventional Shale Gas Reservoirs. *SPE International Oil and Gas Conference and Exhibition*, Beijing, China; 2010.

[20] Jin Z, Firoozabadi A. Thermodynamic Modeling of Phase Behavior in Shale Media. *SPE Journal* 2016; 21(1): 190–207.

[21] Jin Z, Firoozabadi A. Phase behavior and flow in shale nanopores from molecular simulations. *Fluid Phase Equilibria* 2016; 430: 156–68.

[22] Swami V, Settari A. A Pore Scale Gas Flow Model for Shale Gas Reservoir. *SPE Unconventional Resources Conference*, Pittsburgh, USA; 2012.

[23] Guo C, Wu K, Wei M. Study on gas flow through nano pores of shale gas reservoirs. *Fuel* 2015; 143: 107–17.

[24] Ertekin T, Abou-Kasem JH, King GR. *Basic Applied Reservoir Simulation*. Texas: Society of Petroleum Engineers; 2001

[25] Faires JD, Burden RL. Numerical Methods, Cengage Learning, 2003.

[26] Deb KP, Akter F, Imtiaz SY, Hossain ME, Nonlinearity and solution techniques in reservoir simulation: A review, *Journal of Natural Gas Science and Engineering* 2017; 46: 845-64

[27] Noor MA, Waseem M. Some iterative methods for solving a system of nonlenear

equations 2009; 11: 369-75.

[28] Karr CL, Weck B, Freeman LM. Solutions to systems of nonlinear equations via Genetic Algorithm. Engineering Application Artificial Intelligence 1998; 11: 369-75.

[29] Luo YZ, Tang GJ, Zhou LN. Hybrid approach for solving systems of nonlinear equations using luo chaos optimization and quasi-Newton method Applid Soft Computing 2008; 8: 1068-73.

[30] Mo Y, Liu H, Wang Q. Conjugate direction particle swarm optimization solving systems of nonlinear equations. Computers and Mathematics with Applications 2009; 57: 1877-82.

[31] Jaberipour M, Khorram E, Karimi B. Particle swarm algorithm for solving systems of nonlinear equations. Computers and Mathematics with Applications 2011; 62: 566-76.

[32] Wu Y, Pruess K, Persoff P. Gas Flow in Porous Media with Klinkenberg Effects. *Transport in porous Media* 1998; 32(1): 117–37.

[33] Firouzi M, Alnoaimi K, Kovscek A, Wilcox J. Klinkenberg effect on predicting and measuring helium permeability in gas shales. *International Journal of Coal Geology* 2014; 123: 62–68.

[34] Wang H, Marongiu-Porcu M. Impact of shale-gas apparent permeability on production: combined effects of non-darcy flow/gas-slippage, desorption, and geomechanics. *SPE Reservoir Evaluation & Engineering* 2015; 18(4): 495–507.

[35] Javadpour F, McClure F, Naraghi ME. Slip-corrected liquid permeability and its effect on hydraulic fracturing and fluid loss in shale. *Fuel* 2015; 160,:549–59.

[36] Fathi E, Tinni A, Akkutlu IY. Correction to Klinkenberg slip theory for gas flow in nano-capillaries. *International Journal of Coal Geology* 2012; 103,:51–9.

[37] Beskok A, Karniadakis GE, Report: A model for flows in channels, pipes, and ducts at micro and nano scales. *Microscale Thermophysical Engineering* 1999; 3(1): 43–77.

[38] Roy S, Raju R, Chuang HF, Cruden BA, Meyyappan M, Modeling gas flow through microchannels and nanopores. *Journal of Applied Physics* 2003; 93(8): 4870–9.

[39] Ziarani AS, Aguilera R. Knudsen's Permeability Correction for Tight Porous Media. *Transport in porous media* 2012; 91(1): 239–260.

[40] Nazari Moghaddam R, Jamiolahmady M. Slip flow in porous media. *Fuel 2016*; 173: 298–310.

[41] Song W, Yao J, Li Y, Sun H, Zhang L, Yang Y, Zhao J, Sui H, Apparent gas permeability in an organic-rich shale resrvoir. *Fuel* 2016; 181: 973-84.

[42] Geng L, Li G, Zitha P, Tian S, Sheng M, Fan X.A diffusion-viscous flow model for simulating shale gas transport. *Fuel* 2016; 181: 887-94.

[43] Freeman CM, Moridis GJ, Blasingame TA. A Numerical Study of Microscale Flow Behavior in Tight Gas and Shale Gas Reservoir Systems. *Transport in porous media* 2011; 90(1): 253–268.

[44] Wu K, Li X, Wang C, Yu W, Chen Z. Model for surface diffusion of adsorbed gas in nanopores of shale gas reservoirs. *Industrial & Engineering Chemistry Research* 2015; 54(12): 3225–3236.

[45] Heller R, Zoback M. Adsorption of methane and carbon dioxide on gas shale and pure

mineral samples. *Journal of Unconventional Oil and Gas Resources* 2014; 8: 14–24.

[46] Yu W, Sepehrnoori K. Simulation of gas desorption and geomechanics effects for unconventional gas reservoirs. *Fuel* 2014; 116: 455–64.

[47] Yuan W, Pan Z, Li X, Yang Y, Zhao C, Connell LD, Li S, He J. Experimental study and modelling of methane adsorption and diffusion in shale, *Fuel*, 2014, 117, 509–519.

[48] Yu W, Sepehrnoori K, Patzek TW. Modeling Gas Adsorption in Marcellus Shale With Langmuir and BET Isotherms. *SPE Journal* 2016; 21(2): 589-600.

[49] Sakhaee-pour A, Bryant SL. Gas Permeability of Shale. *SPE Reservoir Evaluation & Engineering* 2012; 15(04): 401-9

[50] Singh H, Javadpour F. Langmuir slip-Langmuir sorption permeability model of shale. *Fuel* 2016; 164: 28–37.

[51] Kazemi M, Takbiri-Borujeni A. An analytical model for shale gas permeability. *International Journal of Coal Geology* 2015; 146: 188–197.

[52] Svrcek WY, Mehrotra AK. Gas Solubility, Viscosity and Density Measurements for Athabasca Bitumen. *Journal of Canadian Petroleum Technology* 1982; 21(4): 31–38.

[53] S. R. Etminan, F. Javadpour, B. B. Maini, and Z. Chen, Measurement of gas storage processes in shale and of the molecular diffusion coefficient in kerogen, *International Journal of Coal Geology*, 2014, 123, 10–19.

[54] Huang T, Guo X, Chen F. Modeling transient pressure behavior of a fractured well for shale gas reservoirs based on the properties of nanopores. *Journal of Natural Gas Science and Engineering* 2015; 23: 387–98.

[55] Mi L, Jiang H, Li J. The impact of diffusion type on multiscale discrete fracture model numerical simulation for shale gas. *Journal of Natural Gas Science and Engineering* 2014; 20: 74–81.

[56] Chen F, Duan Y, Wang K, Li X, Liao Y. A novel pressure transient response model considering multiple migration mechanisms in shale gas reservoir. *Journal of Natural Gas Science and Engineering* 2015; 22: 321–34.

[57] Lee J, Wattenbarger RA. *Gas Reservoir Engineering*. 1st ed. Texas: Society of Petroleum Engineers; 1996.

[58] Yu W, Huang S, Sepehrnoori K. Development of a Semi-Analytical Model for Simulation of Gas Production in Shale Gas Reservoirs. Unconventional Resources Technology Conference, Denver, USA; 2014.

[59] T. W. Patzek, F. Male, and M. Marder, Gas Production in the Barnett Shale Obeys a Simple Scaling Theory, *Proceedings of the National Academy of Sciences of the United States of America.*,2013, 110(49), 19731–19736.

[60] Cui G, Liu J, Wei M, Shi R, Elsworth D. Why shale permeability changes under variable effective stresses: New insights. *Fuel* 2018; 213: 55-71.

[61] Cherry J. Optimization strategies for shale gas asset development 2016.

[62] Eberhart R, Kennedy J. A new optimizer using particle swarm optimization. *In Proceeding of the sixth International Symposium on Micro Machine and Human Science* 1995; 1: 39-43.

[63] Ahmadi MA. Neural network based unified particle swarm optimization for prediction of

asphaltene precipitation. *Fluid Phase Equilibria* 2012; 314: 46–51.

[64] Ahmadi MA, Ebadi M, Yazdanpanah A. Robust intelligent tool for estimating dew point pressure in retrograded condensate gas reservoirs: Application of particle swarm optimization, *Journal of Petroleum Science and Engineering* 2014; 123: 7–19.

[65] Ahmadi MA, Zendehboudi S, Dusseault MB, Chatzis I. Evolving simple-to-use method to determine water–oil relative permeability in petroleum reservoirs. *Petroleum* 2016; 2(1): 67–78.

[66] Al-Mudhafar WJ, Dalton CA, Al musabeh MI. Metamodeling via Hybridized Particle Swarm with Polynomial and Splines Regression for Optimization of CO2-EOR in Unconventional Oil Reservoirs. SPE Reservoir Charachtersation and Simulation Conference and Exhibition, Abu Dahbi, UAE; 2017.

[67] Ahmadi MA, Ebadi M, Shokrollahi A, Majidi SJ. Evolving artificial neural network and imperialist competitive algorithm for prediction oil flow rate of the reservoir. *Applied Soft Computing* 2013; 13(2): 1085–1098.

[68] Gazi V, Passino KM. Particle Swarm Optimization. Swarm Stability and Optimization. Springer, Berlin; 2011

[69] Hagoort J. *Fundamentals of gas reservoir engineering*. 1st ed. New York: Elsevier; 1988.

Tables

Table 1: Different flow regimes as a function of Knudsen number (K_n) [8, 37-40]

Knudsen Number (K_n)	Flow Regimes	Remarks
$\boldsymbol{K_n < 10^{-3}}$	Continuum Flow (C)	▪ *Surface velocity* of gas molecule at pore wall is *zero* ▪ Darcy's law is *applicable* ▪ The λ of gas molecules has a *negligible value* in comparison with the pore radius
$\boldsymbol{10^{-3} < K_n < 10^{-1}}$	Slip Flow (S)	▪ The theory of *continuum flow breaks down* ▪ The frequency of molecules' collisions with pore wall is not insignificant anymore
$\boldsymbol{10^{-1} < K_n} < 10$	Transition Flow (T)	▪ Molecules *strike against the pore walls* and lean towards *slipping on pore walls* instead of having zero velocity ▪ λ is in the *comparable magnitude of order* with pore sizes
$\boldsymbol{10 < K_n} < \infty$	Free-Molecular Flow (F)	▪ Molecules travel *more autonomously* from each other ▪ *Collisions* of gas molecules with flow boundaries *occur more repeatedly* in comparison with the inter-molecule collisions

Table 2: Analytical reviews of multi-mechanism apparent permeability models

Model	Correlation	Remarks
Javadpour [4]	$k_{app} = 1.95\frac{r\mu M}{\rho_{avg}^2 T}\left(\frac{T}{M}\right)^{0.5} + 7.9F\frac{r^2}{\rho_{avg}}$ $F = 1 + 1.56\left(\frac{T}{M}\right)^{0.5}\frac{\mu}{P_{avg}r}\left(\frac{2}{\zeta} - 1\right)$	- F is known as the *slip coefficient* - ζ is a function of *pressure*, *temperature*, *gas type* and wall surface *smoothness* - ζ is an *experimental parameter* - ζ is in the *range* of 0 to 1
Darabi et al. [8]	$k_{app} = 31.326\frac{\mu M}{\rho_{avg} T}\frac{\phi}{\tau}(\delta')^{D_f - 2} r\left(\frac{T}{M}\right)^{0.5} + Fk$	- Suitable for a *network of interconnected tortuous* micro pores and nano pores - F is the same as before - ϕ/τ has been introduced to model *Knudsen flow through porous media* - D_f considers effects of *pore surface roughness* as one of the *local heterogeneity* on the Knudsen diffusion - D_f varies between 2 and 3 - δ' is the *ratio size* and defined as d_m/d - $k = \frac{r^2}{8}$

Table 3: Adsorption isotherms routinely used in petroleum industries

Model	Correlation	Remarks
Langmuir [44-47]	$V = V_L \frac{P}{P_L + P}$	- It follows a *stabilized trend at high pressures* - The model is applicable for *all types of surfaces* - The model describes a *mono-layer* of adsorbed gas - It works based on *2 fitting parameters* - Generally known as isotherm of *Type I*
BET [48]	$V_L = \frac{V_m C P}{(P_o - P)\left[1 + \frac{(C-1)P}{P_o}\right]}$	- It is the *general* from of Langmuir isotherm - It follows an *ascending trend at higher pressures* - It is specified for *homogeneous surfaces* - The model describes *multilayer* of adsorbed gas - $C = exp((E_1 - E_L)/RT)$ - It works based on a *couple of fitting parameters* - Generally known as isotherm of *Type II*

Table 4: Effects of adsorbed layer thickness on shale permeability

Model	Correlation	Remarks
Sakhaee-pour and Bryant [49]	$t_{ads} = \alpha P$	- Useful for pores less than 50 nm and organic contents - Thickness of the adsorbed layer is 0.7 nm in pressures above 4061 psi. - α is a fitting slope - Easy to be applied in permeability models - Low computational efforts are required - It is supported with experimental results - The thickness reduces linearly with pressure reduction - Not reflecting the actual thickness of the adsorbed layer
Singh et al. [50]	$t_{ads} = 2r_{mol}$	- Considering molecules are in the sphere shape - $r_{mol} = (3V/4\pi)^{1/3}$ - $V = \frac{ZnRT}{P}$ - It is based on thermodynamical concepts - Huge computational efforts are required

Table 5: PSO parameters [68]

Parameter	**Value**
c_1	2
c_2	2
Number of particles	30
Number of parameters (pressures) in each particle	Number of grids

Table 6: Initial values of parameters [8, 22, 48]

Parameter	Value
Temperature (˚F)	200
Initial Pressure (psi)	5000
C1 %	100
k (md)	0.0008
ϕ	0.14
X (ft)	4
P_{wf} (psi)	400
α	0.8
τ	4
D_f	2.5
P_L (psi)	1240
V_L (ft^3/lb)	0.08015
$\boldsymbol{\rho_b}$(lb/ft^3)	164.185
$\boldsymbol{\rho_g}$(lb/ft^3)	0.04236
D (ft^2/day)	2.15×10^{-10}
k_H (lb/psi-ft^3)	3.2×10^{-4}
Duration (day)	4

Table 7: Effects of complexity versus volume of calculations for both applied solvers (■ is about the computational time of Newton's Method and ■ is about the PSO)

Characteristics	*Number of Grids*				
	100	200	300	400	500
Basic Model	4	11	18	27	38
	4	10	17	25	35
Basic Model + K*app*	8	20	32	50	88
	6	14	24	38	65
Basic Model + K*app* + Desorption	10	25	52	90	130
	8	18	40	69	100
Basic Model + K*app* + Desorption + Effects of Adsorbed Layer	12	30	60	106	151
	8	19	41	77	112
Basic Model + K*app* + Desorption + Effects of Adsorbed Layer + Solute Gas	18	37	70	122	178
	11	23	44	82	124

Figures

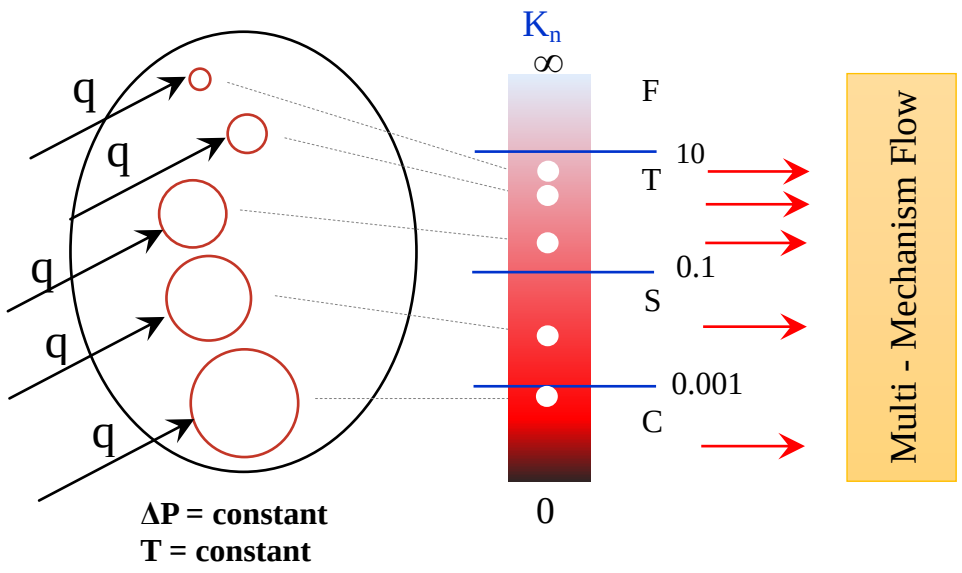

Figure 1: Multi-mechanism flow in a thin section of a shale gas reservoir as a function of K_n

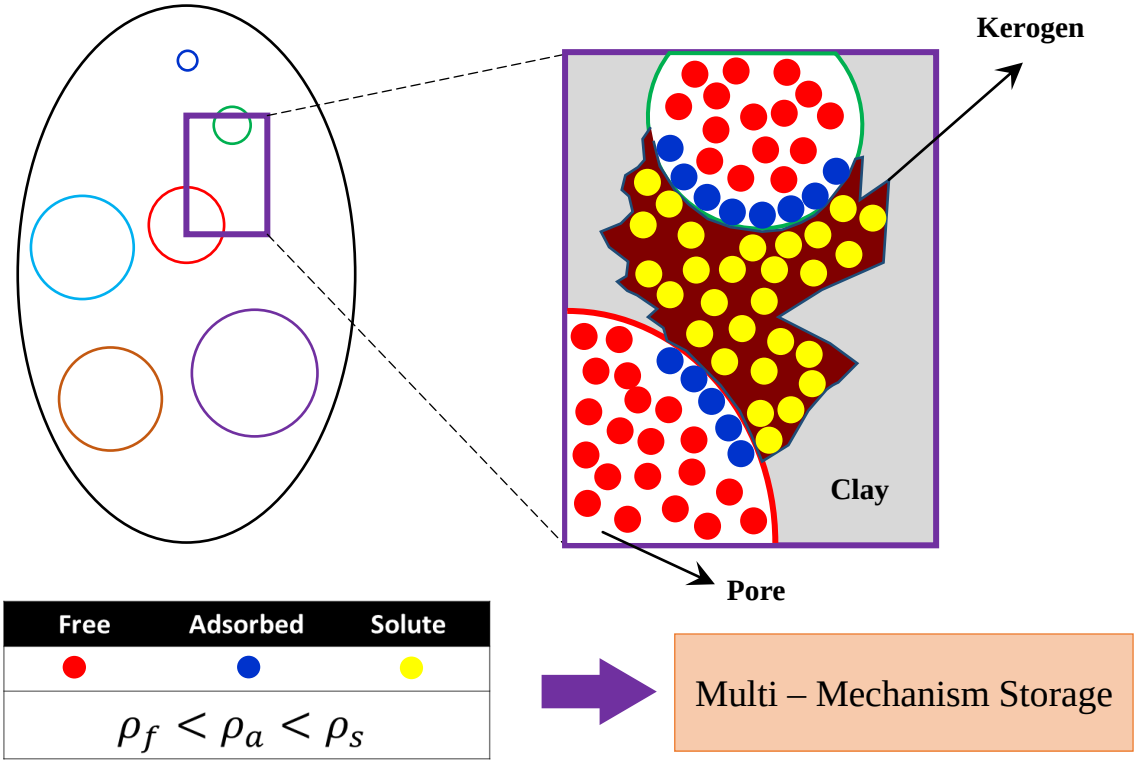

Figure 2: Schematic of storage in a thin section of a shale gas reservoir, different pore sizes have colorfully and schematically been distinguished

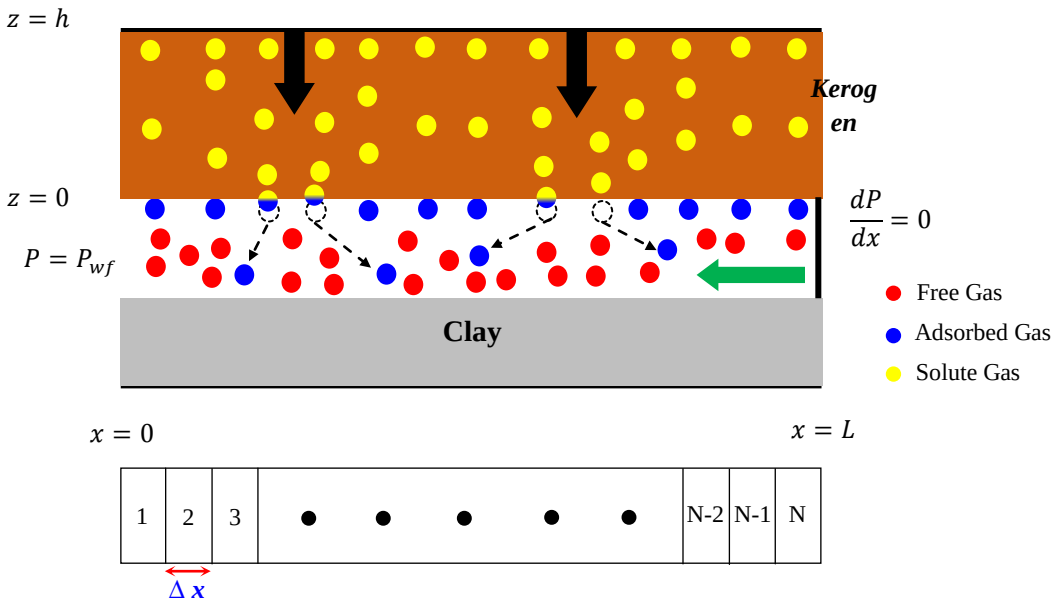

Figure 3: Schematic of the supposed physical model

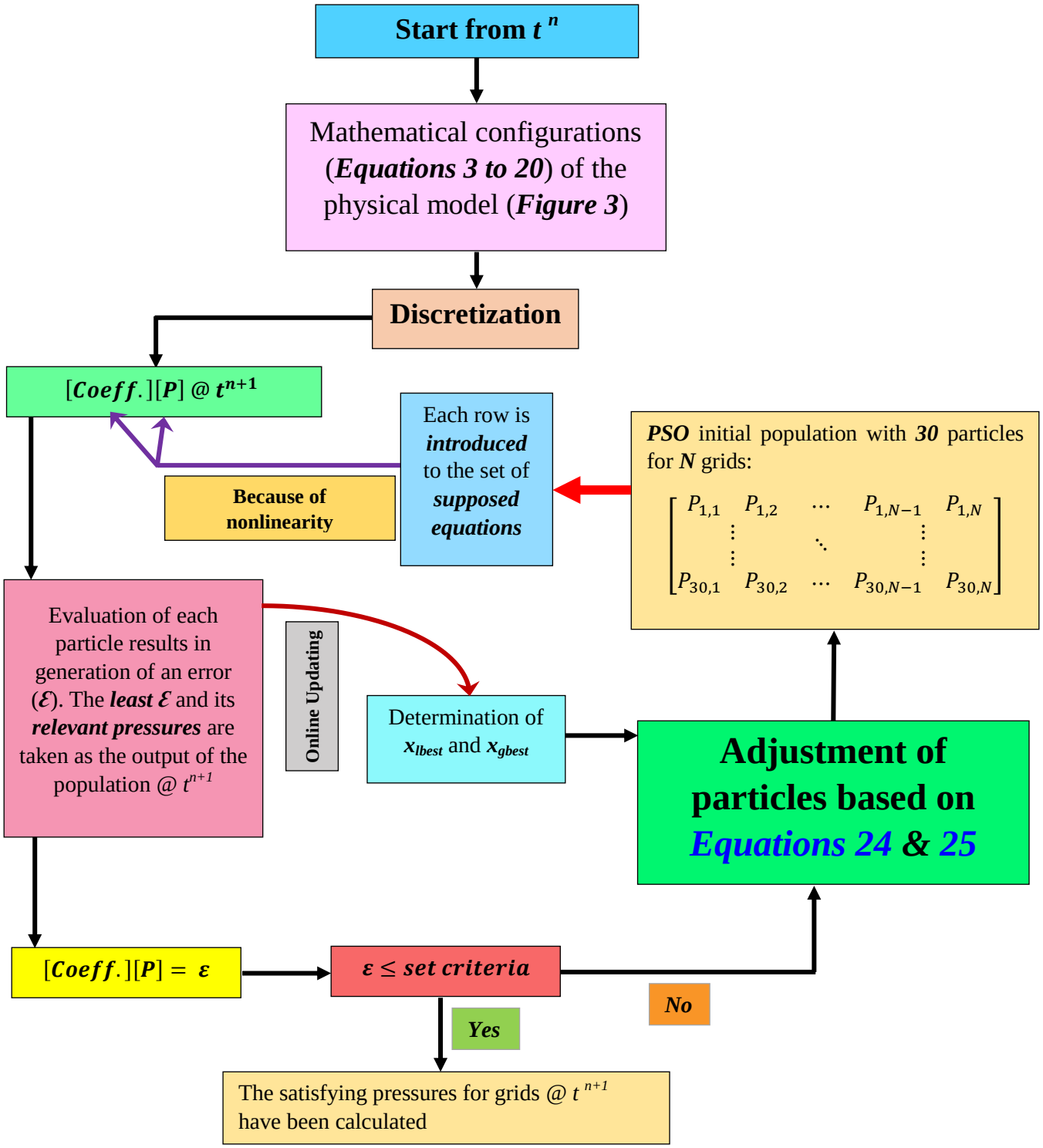

Figure 4: The schematic of the proposed hybrid of PSO and conventional techniques

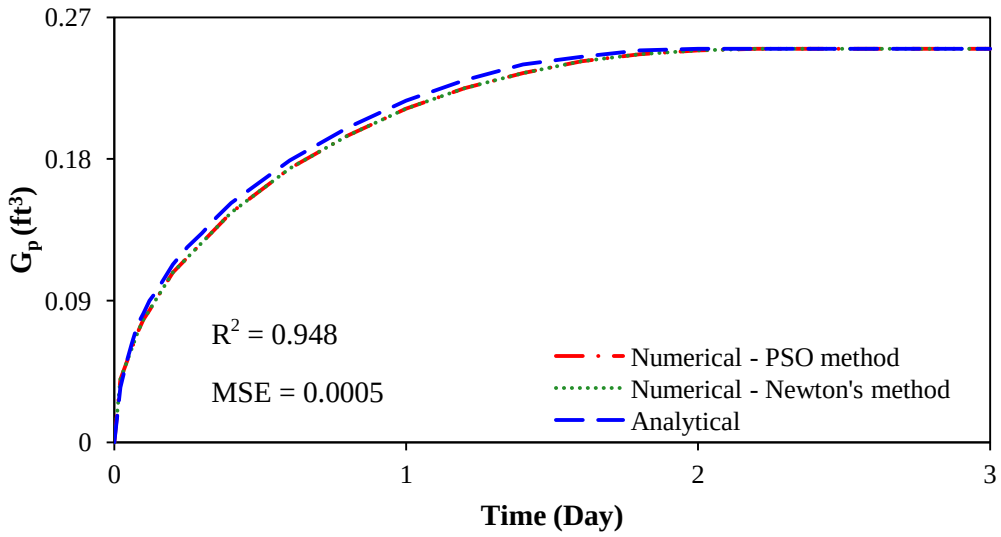

(a)

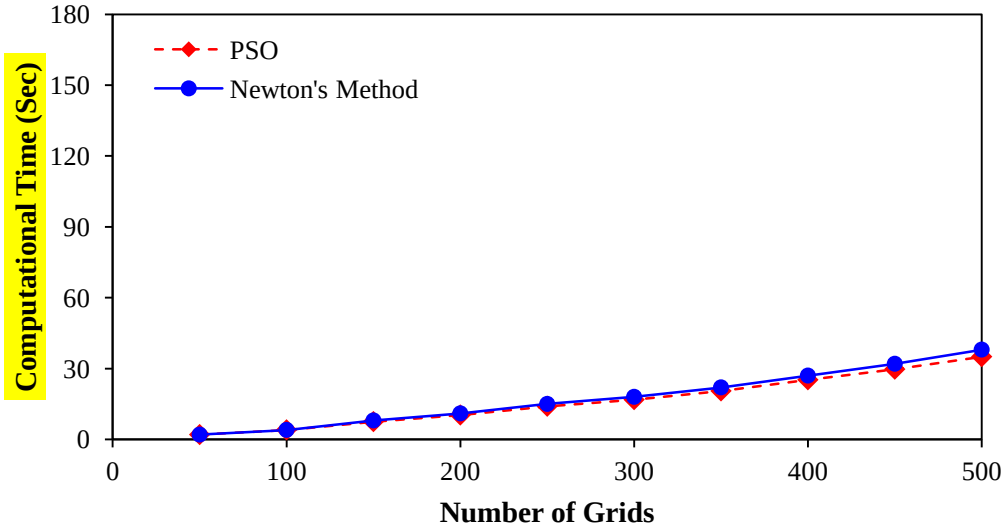

(b)

Figure 5: *(a)* Validation of the applied numerical methods for 300 grids *(b)* Performance of the PSO versus Newton's method to solve corresponding simultaneous equations

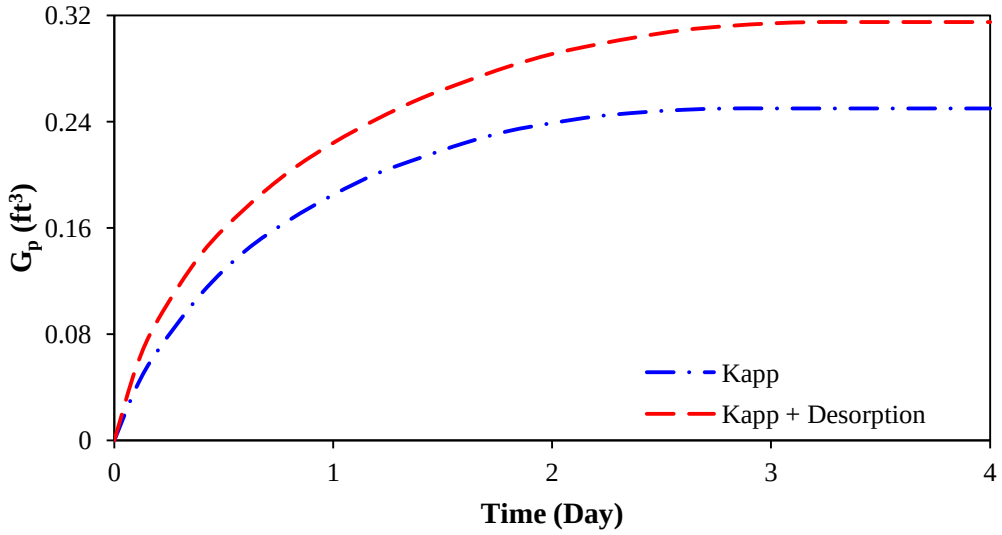

(a)

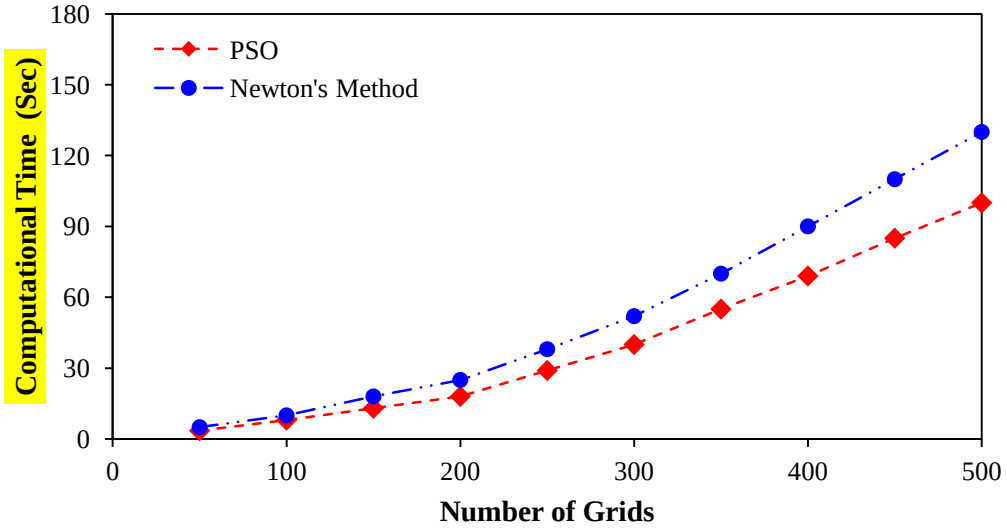

(b)

Figure 6: *(a)* The production profile as a function of the apparent permeability and desorption phenomenon for 300 grids *(b)* Effectiveness of PSO technique to solve a large number of non-linear simultaneous equations with higher levels of complexities

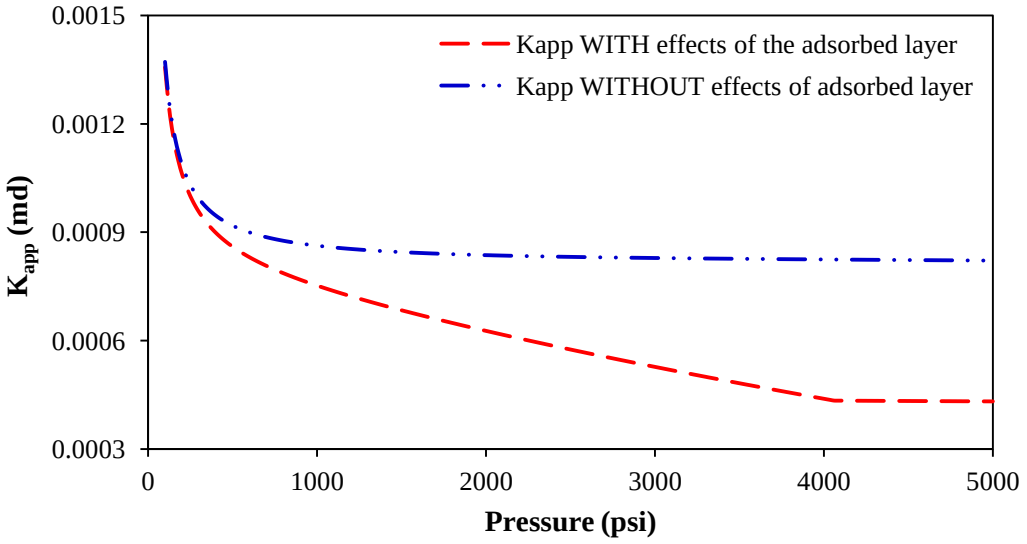
0.0015
0.0012
0.0009
0.0006
0.0003
K_{app} (md)
0
1000
2000
3000
4000
5000
Pressure (psi)
Kapp WITH effects of the adsorbed layer
Kapp WITHOUT effects of adsorbed layer

(a)

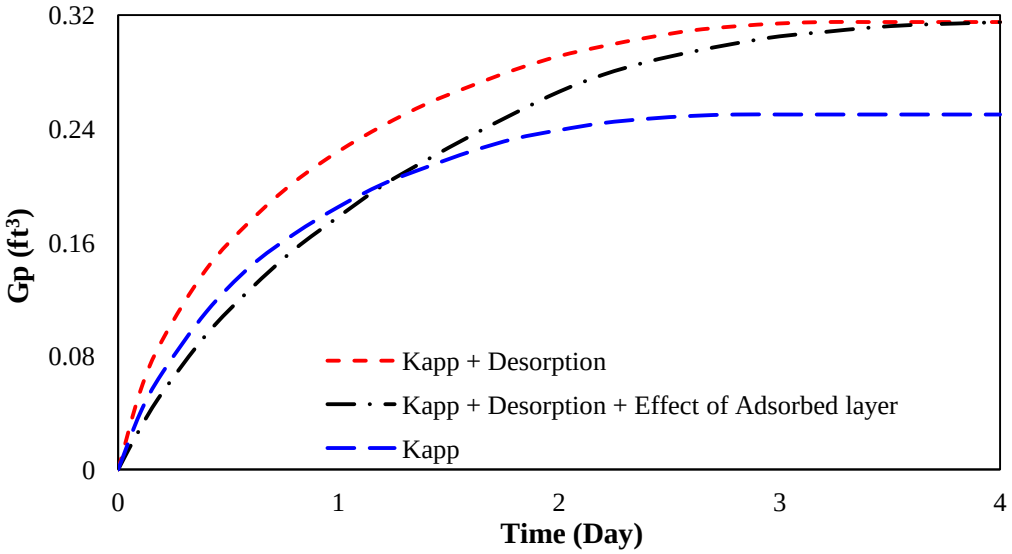
0.32
0.24
0.16
0.08
0
Gp (ft^3)
0
1
2
3
4
Time (Day)
Kapp + Desorption
Kapp + Desorption + Effect of Adsorbed layer
Kapp

(b)

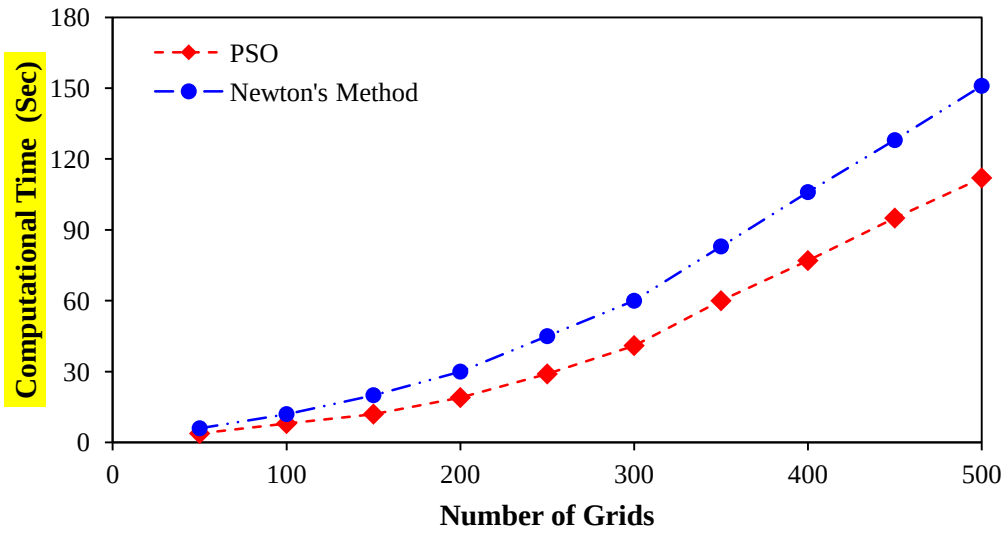

(c)

Figure 7: *(a)* Effects of the adsorbed layer on the values of apparent permeability in different pressures *(b)* Profiles of cumulative production as a function of the adsorbed layer for 300 grids *(c)* PSO method vs. Newton's method in case of including the adsorbed layer effects

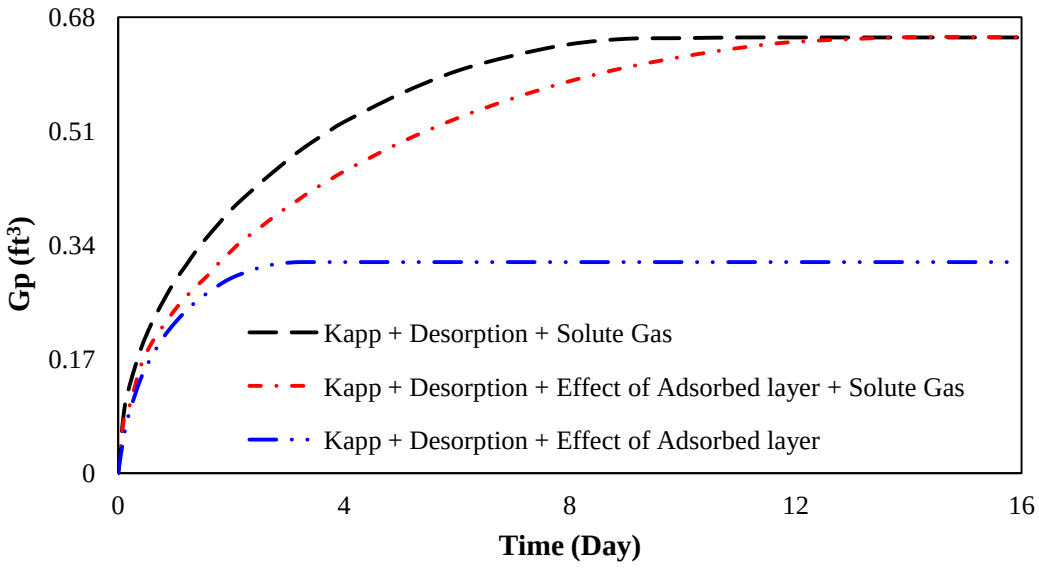

(a)

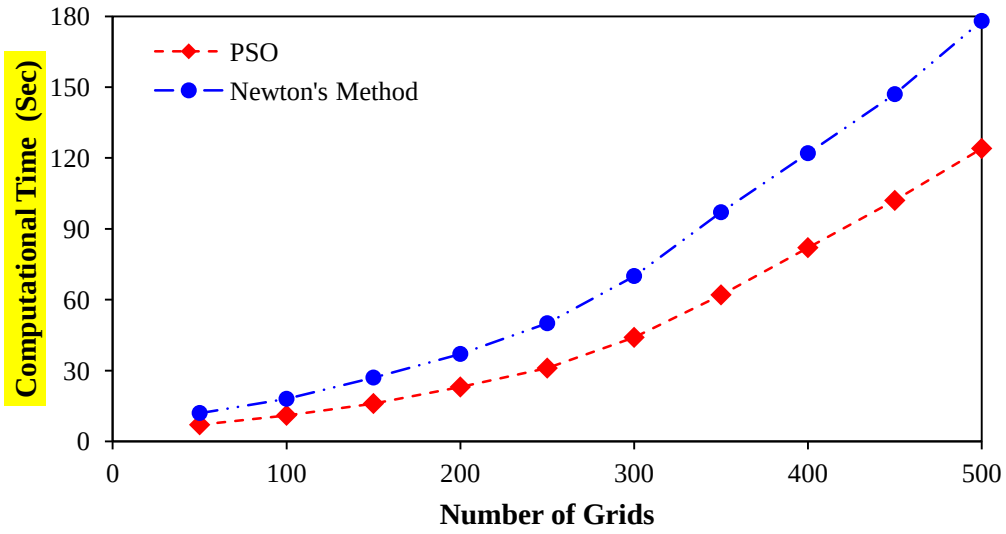

(b)

Figure 8: *(a)* Effects of kerogen inclusion on the trend and value of the cumulative production for 300 grids *(b)* How the PSO can reduce the Computational Time in the most complicated case based on the number of grids

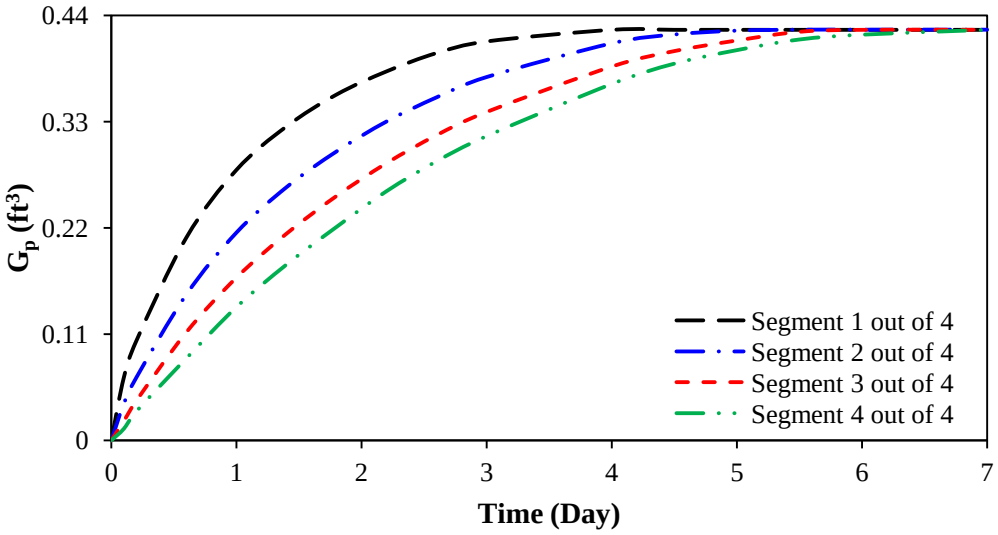

Figure 9: Cumulative production as a function of kerogen distributions for 300 grids